Eur. Phys. J. C (2013) 73:2343
DOI 10.1140/epjc/s10052-013-2343-8

THE EUROPEAN PHYSICAL JOURNAL C

Special Article - Tools for Experiment and Theory

A study of measurement precision of the Higgs boson branching ratios at the International Linear Collider

Hiroaki Ono[1,a], **Akiya Miyamoto**[2]

[1]School of Life Dentistry at Niigata, Nippon Dental University, 1-8 Hamaura-cho, Chuo-ku, Niigata 951-8580, Japan
[2]High Energy Accelerator Research Organization, 1-1 Oho, Tsukuba 305-0801, Japan

Received: 25 September 2012 / Revised: 2 February 2013 / Published online: 8 March 2013

Abstract Precise measurement of the Higgs boson couplings is an important task for International Linear Collider (ILC) experiments and will clarify the understanding of the particle mass generation mechanism. In particular, high precision measurement of Higgs branching ratios plays a key role in the search for the origin of the Yukawa and Higgs interactions. In this study, the measurement accuracies of Higgs boson branching ratios to b and c quarks and gluons were evaluated using a full detector simulation based on the International Large Detector, and assuming a Higgs mass of 120 GeV/c^2. We analyze two center-of-mass (CM) energies, 250 and 350 GeV, close to the $e^+e^- \to ZH$ and $e^+e^- \to t\bar{t}$ production thresholds. At both energies, an integrated luminosity of 250 fb^{-1} and an electron (positron) beam polarization of -80 % ($+30$ %) were assumed. We obtain the following measurement accuracies for the product of the Higgs production cross section and the branching ratio of the Higgs into $b\bar{b}$, $c\bar{c}$, and gg: 1.0 %, 6.9 %, and 8.5 % at a CM energy of 250 GeV and 1.0 %, 6.2 %, and 7.3 % at 350 GeV. (After writing our article, Large Hadron Collider experiments reported the observation of a new resonance around the mass of 125 GeV/c^2 (ATLAS Collaboration, arXiv:1207.7214v1 [hep-ex]; CMS Collaboration, arXiv:1207.7235v1 [hep-ex]). Considering the small difference in branching ratios of the Higgs at masses of 120 and 125 GeV/c^2, our results are not significantly affected by this mass difference.)

1 Introduction

The Higgs boson is a spin-zero particle responsible for the mass generation of elementary particles. In the Standard Model (SM), the Yukawa couplings of the Higgs boson to the fermion fields are given by the ratio of the respective fermion masses to the vacuum expectation value of the Higgs doublet. This relation may however be modified in theories beyond the SM [1]. The Higgs boson has been searched for over many years at several experiments [2–5] and a precise study of Higgs boson properties is a primary target of the future high energy collider, International Linear Collider (ILC).

Precise measurements of the Higgs decay branching ratios (BRs) are crucial to confirm the mass-coupling relation in SM or to search for physics beyond the SM [6–9]. In experiments at the Large Hadron Collider (LHC) [4, 5], it is not easy to measure the BRs of Higgs to quarks and gluons due to the large QCD backgrounds in hadron collisions. In contrast, precise measurements of BRs are anticipated at e^+e^- linear collider experiments, owing to the cleaner experimental conditions, well-defined initial states and beam polarizations [10, 11].

Studies of the measurement of Higgs BRs at linear colliders have been performed at several center-of-mass (CM) energies employing fast detector simulations [12–14], predicting BR precisions ranging from a few percent to $\mathcal{O}(10\ \%)$ for hadronic decay channels. These measurements require good jet energy resolution and efficient quark flavor tagging however the performance of such tools is difficult to simulate reliably in fast simulation tools. A detailed and realistic detector model and sophisticated reconstruction tools are required to make reliable prediction for the achievable precision of such measurements.

Full simulation studies of BRs measurements of Higgs to $b\bar{b}$, $c\bar{c}$ and gg have been reported using the ILD [10] and SiD [11, 15] detector models at a CM energy of 250 GeV. The SiD study was based on a neural net based cut analysis, while the ILD study performed only a simple cut based analysis on a few decay modes. This paper is an extension of the

[a] e-mail: ono@ngt.ndu.ac.jp

ILD analysis including all possible detection channels and employing a template fitting technique for an improved sensitivity. The study also includes an analysis at a CM energy of 350 GeV, suitable for a simultaneous study of the top pair production near threshold and Higgs properties.

After describing the detector model and reconstruction tools in Sect. 2, the event selection is described in the Sect. 3 and the determination of branching ratio by a template fitting method is discussed in Sect. 4. The conclusion is given in Sect. 5.

2 Higgs physics at the ILC

2.1 ILC experiment and Higgs production

The ILC is a proposed electron-positron (e^-e^+) linear collider at an initial CM energy ($\sqrt{s}$) up to 500 GeV, extendable to 1 TeV. The production cross section of the Higgs boson is shown in Fig. 1(a) as a function of the CM energy for a Higgs mass of 120 GeV/c^2. At low CM energies, the Higgs boson is produced primarily through the Higgs-strahlung process $e^+e^- \to ZH$, which has a maximum cross section at around 250 GeV, when the effect of initial state radiation is considered. At $\sqrt{s} = 350$ GeV, the total cross section is reduced, although the contribution of the W/Z fusion process is greater than that at 250 GeV.

The decay BRs of the Higgs boson in the SM are shown as a function of its mass in Fig. 1(b). For a Higgs mass around 120 GeV/c^2, its main decay channel is to $b\bar{b}$ and other hadronic decay channels are also sizable. Higgs analysis modes are categorized in terms of the three Z boson decay channels: $Z \to \nu\bar{\nu}$ (neutrino), $q\bar{q}$ (hadronic), and $\ell^+\ell^-$ (leptonic), as shown in Fig. 2. We assume polarizations of -80 % ($+30$ %) for the initial electrons (positrons), which enhances the Higgs production cross section by 50 % with respect to the case with unpolarized beams.

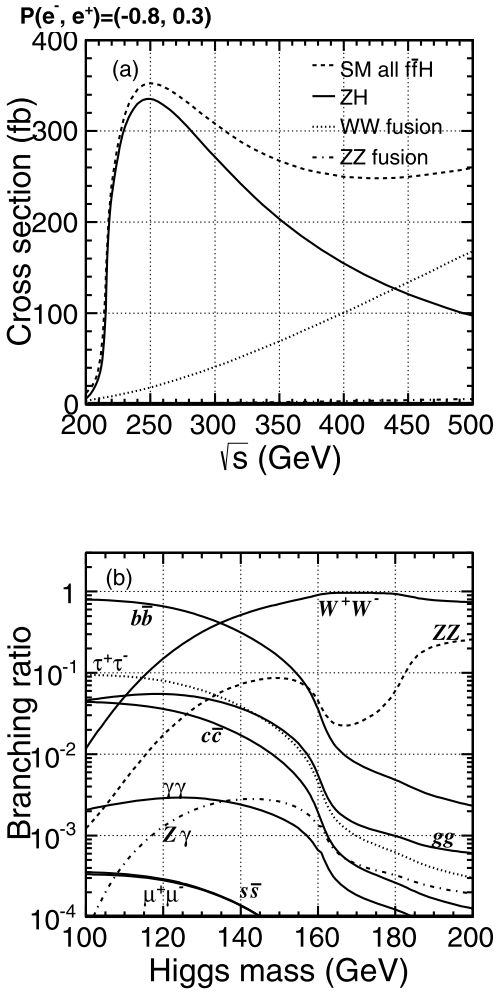

Fig. 1 (**a**) Production cross section of Higgs boson at a Higgs mass of 120 GeV/c^2 through the Higgs-strahlung (ZH) (*solid*) and all $f\bar{f}H$ (*dashed*) processes assuming the -80 % electron and $+30$ % positron beam polarization. The cross section was calculated by `Whizard` [16, 17], including the effects of initial state radiation. (**b**) SM Higgs branching ratios as a function of Higgs mass, as calculated by `PYTHIA` [18]

2.2 ILD concept

We used the ILD model for this study. The ILD is equipped with a highly segmented calorimeter and a hybrid tracking system consisting of gaseous, silicon-strip, and silicon-pixel trackers. They provide an excellent jet energy resolution by the use of particle flow analysis, as well as excellent momentum resolution and vertex flavor tagging capability, necessary for the precision measurement of multi-jet final states in the ILC energy region.

All sub-detector components of the ILD are shown in Fig. 3. The ILD consists of a silicon-pixel vertex detector (VTX), silicon inner and outer detectors (SIT, SET, ETD), a time projection chamber (TPC), high-granularity electromagnetic and hadron calorimeters (ECAL, HCAL), a superconducting solenoid providing a 3.5 T magnetic field, and an iron return yoke with a muon detector. Additional silicon trackers and beam/luminosity calorimeters are installed in the forward region.

The VTX system consists of three double layers of silicon pixel sensors with a 2.8 μm point resolution located at radii between 16 mm and 60 mm, with a total radiation length of 0.74 %. The impact parameter resolution (σ_{IP}) of the VTX system is 5 μm $\oplus$ 10 μm $\cdot$ GeV/$c/p \sin^{3/2}\theta$. The TPC occupies a volume up to a radius of 1.8 m, with a half-length of 2.3 m along the beam axis, providing a stand-alone momentum resolution of $\sigma_{1/P_T} \sim 9 \times 10^{-5}$ GeV^{-1}. The SIT and SET are placed at the inner and outer sides of the TPC, providing a point resolution of 7 (50) μm in the $R-\phi$ (z) direction. The overall momentum resolution of the tracking system (σ_{1/P_T}) is 2×10^{-5} GeV$^{-1} \oplus 1 \times 10^{-3}/P_T \sin\theta$ in

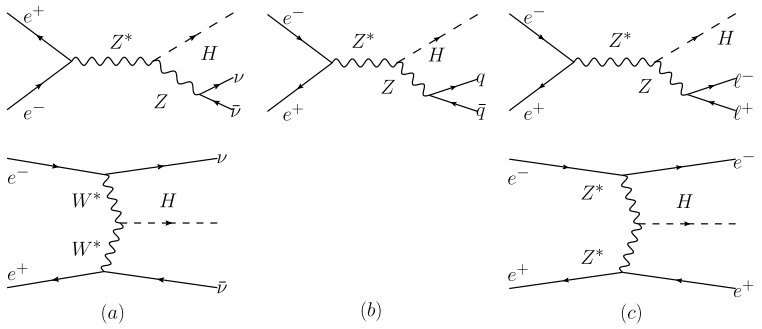

Fig. 2 Higgs boson production diagrams categorized according to the final states: (**a**) neutrino ($\nu\bar{\nu}H$), (**b**) hadronic ($q\bar{q}H$), and (**c**) leptonic ($\ell^+\ell^-H$) channels. Each channel is produced mainly through the Higgs-strahlung (ZH) process at low CM energies, although the neutrino (charged lepton) channels also include contributions from WW (ZZ) fusion

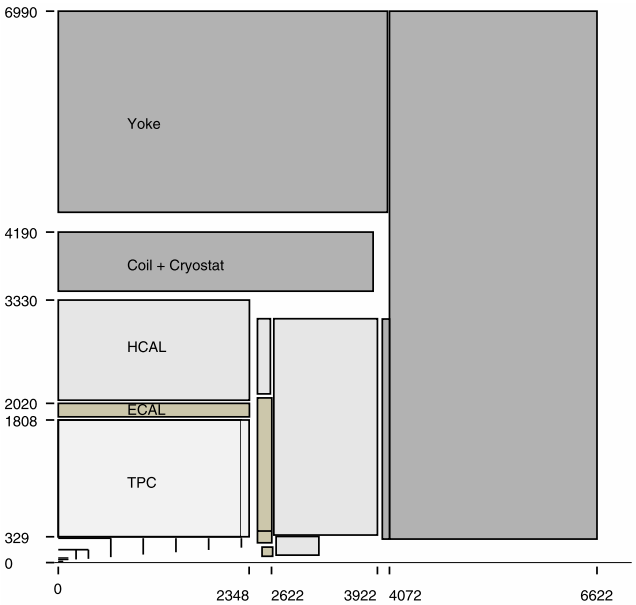

Fig. 3 A schematic view of the ILD detector

the momentum range 1-200 GeV [10]. The ECAL consists of tungsten absorber layer (total thickness of 24 X_0) with a highly segmented (5×5 mm^2) readouts. The HCAL consists of steel absorber layers (total thickness 5.5 λ_I) with a 3×3 cm^2 scintillator tile readout. Using the ILD particle flow algorithm package, `PandoraPFA` [19], a dijet energy resolution of $25\,\%/\sqrt{E\ (\mathrm{GeV})}$ has been achieved for a 45 GeV dijet [10].

2.3 Analysis framework and Monte Carlo samples

Monte Carlo (MC) generator samples for the physics study were produced using `Whizard`. Fragmentation and hadronization processes were simulated by `PYTHIA`. The SM Higgs branching ratios in `PYTHIA` are 65.7 %, 3.6 %, and 5.5 % for $b\bar{b}$, $c\bar{c}$, and gg, respectively. The generated particles were passed through the `Geant4` [20] based detector simulator `Mokka` [21] using the ILD model. The simulated hits were digitized by the MarlinReco package [22], which was also used to reconstruct tracks of charged particles. The individual particles are reconstructed following particle flow concept using the PandoraPFA package. The size of the simulated Higgs signal samples were 500 fb^{-1} for both CM energies of both 250 and 350 GeV. Samples were scaled to obtain results corresponding to an integrated luminosity of 250 fb^{-1}.

The major SM background processes for the $e^+e^- \to ZH$ analysis are $e^+e^- \to ZZ$ and W^+W^-; thus we considered final sample states of $\nu\bar{\nu}q\bar{q}$, $\nu\ell qq$, $\ell\ell q\bar{q}$, $\nu\nu\ell\ell$, $q\bar{q}q\bar{q}$ and $\ell\ell\ell\ell$. In addition, the $q\bar{q}$ and $t\bar{t}$ backgrounds were also considered for the neutrino and hadronic channels. $t\bar{t}$ background was only used for $\sqrt{s} = 350$ GeV generated setting a top mass of 174.9 GeV/c^2 and taking into account the cross section enhancement due to QCD corrections at the top pair threshold [23]. In the leptonic channel, most of the multi-jet backgrounds are very effectively suppressed once dilepton identification is required: in this channel only the $\ell\ell q\bar{q}$ and $\nu\ell qq$ backgrounds were considered.

We used the 250 GeV samples produced for the ILD letter of intent (LOI) studies [10]; thus, their beam parameters correspond to those defined in the ILC Reference Design Report [24]. On the other hand, the 350 GeV samples were produced for this study using the SB2009 [25] beam parameter. The instantaneous luminosities are 0.75 (1) $\times$ (10^{34} cm^{-2} s^{-1}) for 250 (350) GeV, which yield integrated luminosities of 188 (250) fb^{-1} in 300 days of operation at design performance.

3 Event reconstruction and background suppression

Depending on the Z decay mode, the analysis channels are categorized as neutrino (dijet), hadronic (four-jets) or leptonic channels (dileptons+dijets), each of which are described in the following subsections.

3.1 Neutrino channel ($\nu\bar{\nu}H$)

For neutrino channel analysis, particles in the event are first forcibly clustered into two jets by the Durham jet-finding algorithm. After this dijet clustering, selection cuts are applied to reduce backgrounds as shown in Table 1. At a CM energy of 250 GeV, the Higgs is produced almost at rest since it is close to the production threshold, whereas it is boosted at 350 GeV. The cut conditions are therefore optimized to obtain the best signal significance at each energy. In this channel, the Z boson decays invisibly ($\nu\bar{\nu}$), so the $\nu\bar{\nu}q\bar{q}$ and $\nu\ell qq$ processes are the major SM backgrounds. To reduce them, a cut on the missing mass (M_{miss}) was applied. Although this cut decreases the Higgs signal from the WW fusion process, the $\nu\ell qq$, $\ell\ell q\bar{q}$ and $q\bar{q}q\bar{q}$ backgrounds are effectively reduced. The $q\bar{q}$ background was reduced by the following cuts on kinematical variables: the transverse visible momentum (P_t), longitudinal visible momentum (P_l), and maximum track momentum (P_{max}). The $\ell\ell\ell\ell$ background is strongly reduced by a cut on the number of charged tracks in an event (N_{chd}). In addition, the $\nu\ell qq$ background reduction is further reduced by cuts on Y_{12} and Y_{23}, where Y_{12} and Y_{23} are the maximum and the minimum y values (scaled jet masses) required to cluster the event into two jets.

The background reductions for each cut are summarized in Table 1 for each CM energy. After all selection criteria were met, a likelihood ratio (LR) cut was applied to improve the background reduction. The LR was defined using the following variables: M_{miss}, the number of reconstructed particles (N_{PFO}), Y_{12}, P_{max}, P_ℓ, and M_{jj}. The likelihood cut values were optimized to maximize the signal significance, giving $LR > 0.165$ (0.395) at the CM energies of 250 (350) GeV. The signal significance $S/\sqrt{S+B}$ and signal efficiency after all background reductions are also listed in Table 1, where S and B are the numbers of Higgs signal and background events, respectively. The major remaining backgrounds are $\nu\ell qq$ (60 %), $\nu\bar{\nu}q\bar{q}$ (20 %), and $q\bar{q}$ (10 %) at both 250 and 350 GeV.

3.2 Hadronic channel ($q\bar{q}H$)

For the analysis in the hadronic channel, particles in the event are first forcibly clustered into four jets with Durham algorithm. These jets were then paired into Higgs and Z candidate dijets that minimize the following χ^2:

$$\chi^2 = \left(\frac{M_{j_1 j_2} - M_Z}{\sigma_Z}\right)^2 + \left(\frac{M_{j_3 j_4} - M_H}{\sigma_H}\right)^2, \quad (1)$$

where $M_{j_1 j_2/j_3 j_4}$ represent the dijet invariant masses paired from the four jets (j_{1-4}), and $M_{Z/H}$ are the Z and Higgs masses. Here $\sigma_Z = 4.7$ GeV and $\sigma_H = 4.4$ GeV were used for $\sqrt{s} = 250$ GeV and $\sigma_{Z/H} = 3.8$ GeV for $\sqrt{s} = 350$ GeV. These resolutions were determined from the dijet mass distribution reconstructed using the true MC information, as shown in Fig. 4. After the jet pairing, background reduction cuts were applied.

To select the four-jet-like events, cuts on the number of charged tracks $N_{charged}$ and jet clustering parameter Y_{34} were applied. Y_{34} is the minimum scaled jet mass y required for four-jet clustering. The leptonic backgrounds ($\ell\ell\ell\ell$, $\ell\ell q\bar{q}$) are effectively reduced by these conditions. In addition, cuts on the thrust and thrust angle were applied to reduce the ZZ background, utilizing the difference between the event shape of the signal (isotropic) and ZZ, $q\bar{q}$ (back-to-back). The numbers of $q\bar{q}q\bar{q}$ and $q\bar{q}$ background events were reduced by a cut on the angle between the Higgs candidate jets (θ_H). The WW and ZZ backgrounds are further suppressed by cuts on the results of a kinematical constrained fit to the four-jet system, performed as follows: each

Table 1 Summary of the $\nu\bar{\nu}H$ channel background reduction assuming $\mathscr{L} = 250\ \text{fb}^{-1}$ with $P(e^-, e^+) = (-0.8, +0.3)$

CM energy	250 GeV			350 GeV		
Cut names	Condition	Sig.	Bkg.	Condition	Sig.	Bkg.
Generated		19360	44827100		26307	20855900
Missing mass	$80 < M_{miss} < 140$ GeV	15466	6214050	$50 < M_{miss} < 240$ GeV	23202	5627040
Transverse visible momentum	$20 < P_T < 70$ GeV	13727	549340	$10 < P_T < 140$ GeV	22648	2271090
Longitudinal visible momentum	$P_L < 60$ GeV	13342	392401	$P_L < 130$ GeV	22459	2051010
# of charged tracks	$N_{chd} > 10$	12936	374877	$N_{chd} > 10$	21270	1936220
Maximum track momentum	$P_{max} < 30$ GeV	11743	205038	$P_{max} < 60$ GeV	20556	1167050
Y_{23} value	$Y_{23} < 0.02$	7775	74439	$Y_{23} < 0.02$	14992	465461
Y_{12} value	$0.2 < Y_{12} < 0.8$	7438	62584	$0.2 < Y_{12} < 0.8$	14500	413762
Di-jet mass	$100 < M_{jj} < 130$ GeV	6691	19061	$100 < M_{jj} < 130$ GeV	12334	71918
Likelihood ratio	$LR > 0.165$	6293	10940	$LR > 0.395$	9543	11092
Significance (Efficiency)	$S/\sqrt{S+B}$	47.9 (32.5 %)		$S/\sqrt{S+B}$	66.4 (36.3 %)	

jet was parameterized by E_{j_i}, θ_i, and ϕ_i ($i = 1$–4) and fitted with constraints on the total energy ($\sum_i E_{j_i} = \sqrt{s}$), the total momentum ($\sum_i \mathbf{P}_{j_i} = 0$), and Higgs and Z mass difference ($M_{j_1 j_2} - M_{j_3 j_4} = M_H - M_Z$), where E_{j_i}, P_{j_i}, θ_i, and ϕ_i are the energy, momentum, and theta and phi angles of the i-th jet, respectively. After these cuts were applied, an additional cut was applied on a LR derived from the following input variables: thrust, $\cos\theta_{thrust}$, minimum angle between all jets (θ_{min}), number of particles in Higgs candidate jets, fitted Z mass, and fitted Higgs mass. The likelihood cut position was selected to maximize the signal significance: $LR > 0.375$ at 250 GeV and $LR > 0.15$ at 350 GeV. All background reduction cuts are summarized in Table 2. The composition of the remaining background after all cuts is 80 % $q\bar{q}q\bar{q}$ and 20 % $q\bar{q}$ at 250 GeV and 60 % $q\bar{q}q\bar{q}$, 30 % $q\bar{q}$ and 10 % $t\bar{t}$ at 350 GeV.

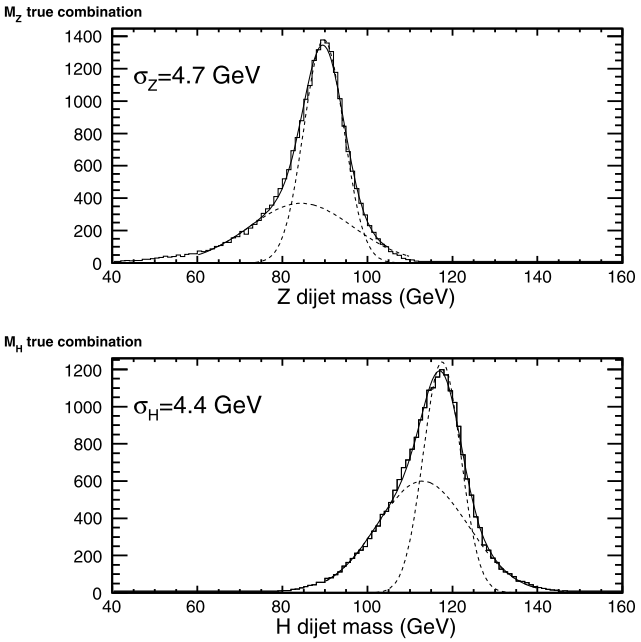

Fig. 4 Reconstructed Z and Higgs dijet mass distribution with true MC jet combination at $\sqrt{s} = 250$ GeV

3.3 Leptonic channel ($\ell^+\ell^- H$)

For the analysis of leptonic channel analysis, we considered the cases where the lepton is either an electron or muon. We considered only the $\ell\ell qq$ and $\ell\nu qq$ background processes. First, the following cuts were applied to selected isolated leptons:

– Lepton isolation: $E_{cone} < 20$ GeV,
– Lepton track momentum:

$$10 < E_{lep} < 90 \text{ GeV} \quad \text{at } \sqrt{s} = 250 \text{ GeV},$$
$$10 < E_{lep} < 160 \text{ GeV} \quad \text{at } \sqrt{s} = 350 \text{ GeV},$$

where E_{cone} is the energy sum for particles within 10 degrees of the lepton. Prompt leptons have a smaller E_{cone} than leptons produced in heavy quark decays. Electrons and muons were identified as follows:

– Electron ID: $\frac{E_{ECAL}}{E_{Total}} > 0.9$, $0.7 < \frac{E_{Total}}{P} < 1.2$
– Muon ID: $\frac{E_{ECAL}}{E_{Total}} < 0.5$, $\frac{E_{Total}}{P} < 0.4$,

where E_{ECAL}, E_{Total} and P denote the ECAL energy associated with a track, total energy deposited in the ECAL and HCAL, and track momentum, respectively. If more than two isolated electron or muon candidates were identified, the pair whose invariant mass is closest to Z is selected.

After the dilepton identification, forced two-jets clustering is applied to the remaining particles and the following selection was applied. First, a dilepton mass ($M_{\ell\ell}$) cut, which should be consistent with the Z mass, was applied: $70 < M_{\ell\ell} < 110$ GeV for electrons and $70 < M_{\ell\ell} <$

Table 2 Summary of $q\bar{q}H$ channel background reduction assuming $\mathscr{L} = 250$ fb^{-1} with $P(e^-, e^+) = (-0.8, +0.3)$

CM energy	250 GeV			350 GeV		
Cut names	Condition	Sig.	Bkg.	Condition	Sig.	Bkg.
Generated		52507	45904900		36099	22210900
χ^2	$\chi^2 < 10$	32447	2608980	$\chi^2 < 10$	20207	1034810
# of charged tracks	$N_{chd} > 4$	25281	1120950	$N_{chd} > 4$	14900	305649
Y_{34} value	$-\log(Y_{34}) > 2.7$	25065	1002125	$-\log(Y_{34}) > 2.7$	14543	250995
thrust	thrust < 0.9	24688	935950	thrust < 0.85	13522	144560
thrust angle	$\lvert\cos\theta_{thrust}\rvert < 0.9$	21892	696201	$\lvert\cos\theta_{thrust}\rvert < 0.9$	12523	107025
Higgs jets angle	$105° < \theta_H < 160°$	20062	622143	$70° < \theta_H < 120°$	11185	77659
Z di-jet mass	$80 < M_Z < 100$ GeV	16359	411863	$80 < M_Z < 100$ GeV	9468	45671
H di-jet mass	$105 < M_H < 130$ GeV	16359	411863	$105 < M_H < 130$ GeV	9451	44399
Likelihood ratio	$LR > 0.375$	13726	166807	$LR > 0.15$	8686	25393
Significance (Efficiency)	$S/\sqrt{S+B}$	32.3 (26.1 %)		$S/\sqrt{S+B}$	47.1 (24.1 %)	

Table 3 Summary of background reduction in the eeH and $\mu\mu H$ channels assuming $\mathscr{L} = 250\ \text{fb}^{-1}$ with $P(e^-, e^+) = (-0.8, +0.3)$

CM energy		250 GeV			350 GeV		
Cut names	e/μ	Condition	Sig.	Bkg.	Condition	Sig.	Bkg.
Generated	e		3137	4512520		2740	3822410
	μ		2917	4512520		1789	3822410
# of e/μ track ID	e	$N_e \geq 2$	2717	204403	$n_e \geq 2$	2270	179580
	μ	$N_\mu \geq 2$	2668	28175	$N_\mu \geq 2$	1631	23598
Di-lepton mass	e	$70 < M_{\ell\ell} < 110$ GeV	2208	34162	$70 < M_{\ell\ell} < 110$ GeV	1425	51436
	μ	$80 < M_{\ell\ell} < 110$ GeV	2287	12901	$80 < M_{\ell\ell} < 100$ GeV	1406	13313
Z direction	e	$\lvert\cos\theta_Z\rvert < 0.8$	1797	21600	$\lvert\cos\theta_Z\rvert < 0.8$	1192	20874
	μ	$\lvert\cos\theta_Z\rvert < 0.8$	1889	8036	$\lvert\cos\theta_Z\rvert < 0.8$	1203	6250
Di-jet mass	e	$100 < M_{jj} < 140$ GeV	1394	2721	$110 < M_{jj} < 140$ GeV	865	2019
	μ	$115 < M_{jj} < 140$ GeV	1445	1955	$115 < M_{jj} < 140$ GeV	855	1197
Recoil mass	e	$70 < M_{rec} < 140$ GeV	1184	1607	$70 < M_{rec} < 140$ GeV	567	590
	μ	$70 < M_{rec} < 140$ GeV	1365	983	$70 < M_{rec} < 140$ GeV	638	465
Significance (Efficiency)	e	$S/\sqrt{S+B}$	22.4 (37.8 %)		$S/\sqrt{S+B}$	16.7 (20.7 %)	
	μ		28.2 (46.8 %)			19.2 (35.7 %)	

100 GeV for muons. Because the ZZ or WW backgrounds are boosted to the forward region compared to the signal, a cut was applied on the polar angle of the Z momentum: $|\cos\theta_Z| < 0.8$. Finally, cuts on dijet mass (M_{jj}) and the mass recoil to the lepton pair (M_{rec}) were applied to select the Higgs signal: $100 < M_{jj} < 140$ GeV and $70 < M_{rec} < 140$ GeV for electrons; $115 < M_{jj} < 140$ GeV and $70 < M_{rec} < 140$ GeV for muons. The background reduction procedures for the leptonic channel are summarized in Table 3. After all cuts were applied, the background was dominated by $\ell\ell q\bar{q}$.

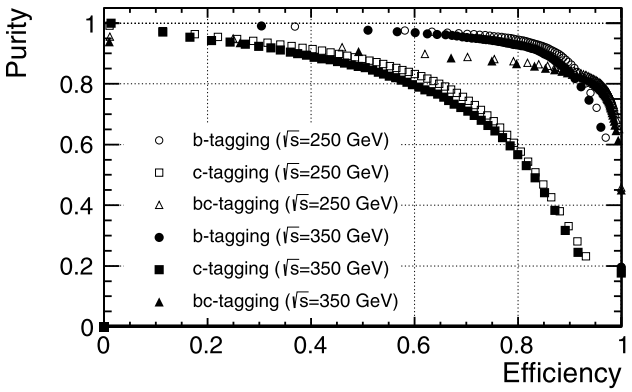

Fig. 5 Flavor tagging performance at CM energies of 250 and 350 GeV in the $ZZ \to \nu\bar{\nu}q\bar{q}$ sample. The *horizontal axis* shows the efficiency for b/c jets; *vertical axis* shows the purity of tagged b/c jets

4 Branching ratio measurement

After the event selection, the measurement accuracies of the Higgs BRs to $b\bar{b}$, $c\bar{c}$, and gg were evaluated on the basis of template fitting to the flavor likeness of the Higgs dijets, calculated by the LCFIVertexing package [26]. The probabilities of b and c quarks for each jet $[b_i, c_i\ (i = 1, 2)]$ were calculated by LCFIVertex using neural networks trained on $Z \to q\bar{q}$ samples generated at the Z-pole. An additional c probability ($bc_{1,2}$) was also calculated, whose neural-net is trained using only the $Z \to b\bar{b}$ sample as background. For Higgs dijets, we define the flavor likeness X ($X = b, c, bc$) as follows from the x_i $[x_i = b_i, c_i, bc_i\ (i = 1, 2)]$ flavor probability of each jet:

$$X = \frac{x_1 x_2}{x_1 x_2 + (1 - x_1)(1 - x_2)}. \tag{2}$$

The flavor tagging performance in the $ZZ \to \nu\bar{\nu}q\bar{q}$ sample at $\sqrt{s} = 250$ and 350 GeV is shown in Fig. 5. The $ZZ \to \nu\bar{\nu}q\bar{q}$ samples are compared for each CM energy because they form the same final state as $Z \to q\bar{q}$, which was used to train the flavor tagging neural networks.

Figure 5 shows that no significant difference in the flavor tagging performance at $\sqrt{s} = 250$ and 350 GeV is observed for any of the flavors.

To evaluate the measurement accuracy of the BRs, the b-, c-, and bc-likenesses of the selected events were binned in a three-dimensional histogram and fitted with those of the template samples, which consist of $H \to b\bar{b}$, $c\bar{c}$, and gg and other background processes. Figure 6 shows the three-dimensional histogram projected to the two-dimensional b- and c-likeness axes for the hadronic channel. The probabil-

ity of entries in each template sample bin is expected to be given by the Poisson statistics:

$$P_{ijk} = \frac{\mu^n e^{-\mu}}{n!} \quad \left(n \equiv N_{ijk}^{data}, \mu \equiv N_{ijk}^{template}\right), \tag{3}$$

where P_{ijk} and N_{ijk}^{data} are the probability of entries and the number of data entries at the (i, j, k) bin, respectively. $N_{ijk}^{template}$ is given by

$$N_{ijk}^{template} = \sum_{s=b\bar{b},c\bar{c},gg} r_s \cdot N_{ijk}^{s} + N_{ijk}^{bkg}, \tag{4}$$

where N_{ijk}^{s} is the number of entries at the (i, j, k) bin in each $H \to b\bar{b}$, $c\bar{c}$, and gg template; N_{ijk}^{bkg} is the number of entries in the background template sample, which is the sum of the SM background events and the Higgs-to-nonhadronic decay events. $r_{b\bar{b}}$, $r_{c\bar{c}}$, and r_{gg} are the parameters to be determined by template fitting. They are defined as the Higgs branching ratios to $H \to b\bar{b}$, $c\bar{c}$ and gg, respectively, normalized SM BRs,

$$r_s = \frac{\sigma \cdot BR(H \to s)}{\sigma^{SM} \cdot BR(H \to s)^{SM}} \ (s = b\bar{b}, c\bar{c}, gg). \tag{5}$$

Here σ is the measured Higgs production cross section and σ^{SM} and $BR(H \to s)^{SM}$ are respectively the cross section and branching ratio in the SM. From Eq. (5), the measurement accuracies of $\sigma \cdot BR$ are obtained as follows;

$$\frac{\Delta(\sigma \cdot BR)}{\sigma \cdot BR}(H \to s) = \frac{\Delta r_s}{r_s} \ (s = b\bar{b}, c\bar{c}, gg).$$

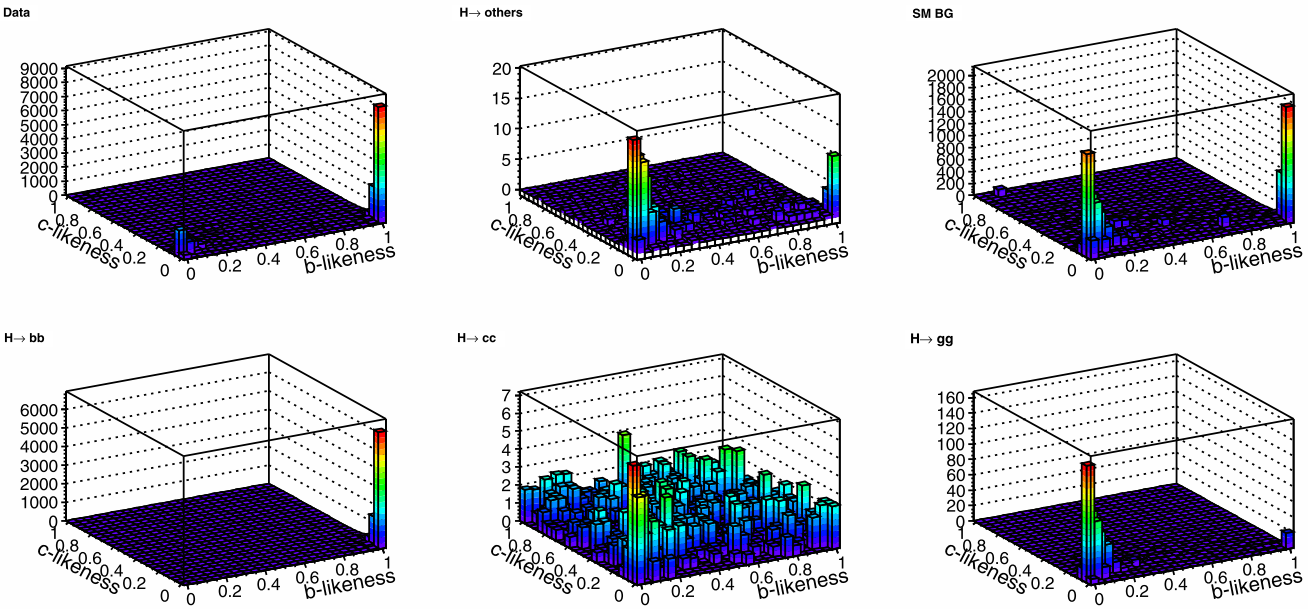

Fig. 6 Two-dimensional projections of three-dimensional template for b-likeness vs. c-likeness

Table 4 Summary of template fitting results r_s and accuracies of $(\sigma \cdot BR)$ and BR after correcting σ for an accuracy of 2.5 % at $\sqrt{s} = 250$ GeV assuming $\mathscr{L} = 250\ \text{fb}^{-1}$ with $P(e^-, e^+) = (-0.8, +0.3)$

	$\nu\bar{\nu}H$	$q\bar{q}H$	e^+e^-H	$\mu^+\mu^-H$	Comb.
$r_{b\bar{b}}$	1.00 ± 0.02	1.00 ± 0.01	1.00 ± 0.04	1.00 ± 0.03	1.00 ± 0.01
$r_{c\bar{c}}$	1.02 ± 0.11	1.01 ± 0.10	1.02 ± 0.27	1.01 ± 0.23	1.02 ± 0.07
r_{gg}	1.02 ± 0.14	1.02 ± 0.13	1.05 ± 0.33	1.02 ± 0.24	1.02 ± 0.09
$\frac{\Delta(\sigma \cdot BR)}{\sigma \cdot BR}(H \to b\bar{b})$ (%)	1.7	1.5	3.8	3.3	1.0
$\frac{\Delta(\sigma \cdot BR)}{\sigma \cdot BR}(H \to c\bar{c})$ (%)	11.2	10.2	26.8	22.6	6.9
$\frac{\Delta(\sigma \cdot BR)}{\sigma \cdot BR}(H \to gg)$ (%)	13.9	13.1	31.3	33.0	8.5
$\frac{\Delta BR}{BR}(H \to b\bar{b})$ (%)	3.0	2.9	5.7	4.5	2.7
$\frac{\Delta BR}{BR}(H \to c\bar{c})$ (%)	11.4	10.5	31.3	22.8	7.3
$\frac{\Delta BR}{BR}(H \to gg)$ (%)	14.2	13.3	33.1	24.0	8.9

Table 5 Summary of template fitting results r_s and accuracies of $(\sigma \cdot BR)$ and BR after correcting σ for an accuracy of 3.5 % at $\sqrt{s} = 350$ GeV assuming $\mathscr{L} = 250$ fb^{-1} with $P(e^-, e^+) = (-0.8, +0.3)$

	$\nu\bar{\nu}H$	$q\bar{q}H$	e^+e^-H	$\mu^+\mu^-H$	Comb.
$r_{b\bar{b}}$	1.00 ± 0.01	1.00 ± 0.02	1.00 ± 0.05	1.00 ± 0.05	1.00 ± 0.01
$r_{c\bar{c}}$	1.02 ± 0.11	1.01 ± 0.10	1.02 ± 0.31	1.04 ± 0.32	1.01 ± 0.06
r_{gg}	1.02 ± 0.14	1.04 ± 0.14	1.04 ± 0.37	1.03 ± 0.34	1.02 ± 0.07
$\frac{\Delta(\sigma \cdot BR)}{\sigma \cdot BR}(H \to b\bar{b})$ (%)	1.4	1.5	5.3	5.1	1.0
$\frac{\Delta(\sigma \cdot BR)}{\sigma \cdot BR}(H \to c\bar{c})$ (%)	8.6	10.1	30.5	30.9	6.2
$\frac{\Delta(\sigma \cdot BR)}{\sigma \cdot BR}(H \to gg)$ (%)	9.2	13.7	35.8	33.0	7.3
$\frac{\Delta BR}{BR}(H \to b\bar{b})$ (%)	3.8	3.8	6.4	6.2	3.6
$\frac{\Delta BR}{BR}(H \to c\bar{c})$ (%)	9.2	10.6	30.7	31.1	7.2
$\frac{\Delta BR}{BR}(H \to gg)$ (%)	9.8	14.1	36.0	33.2	8.1

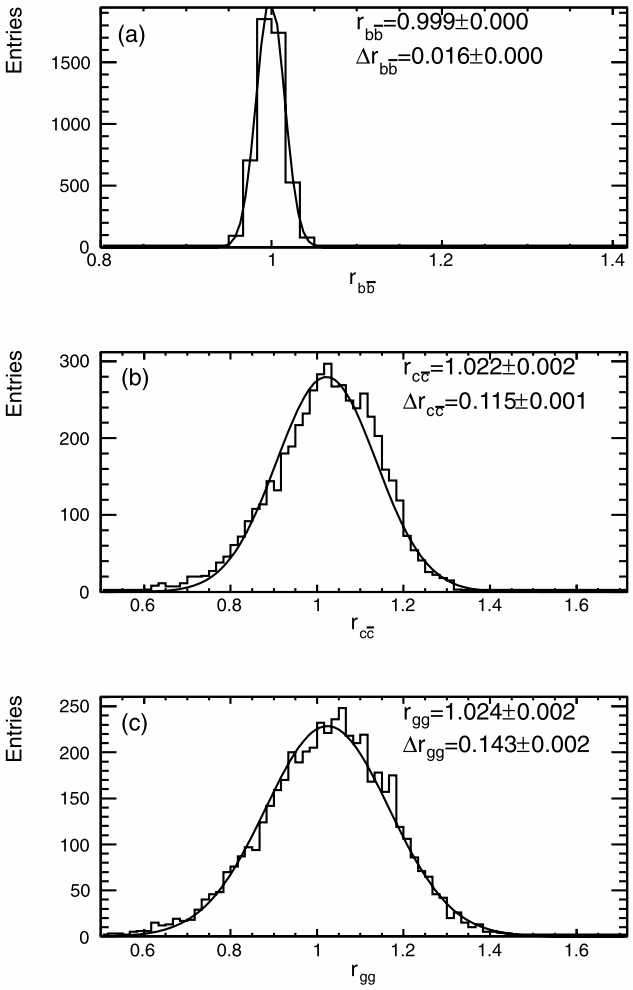

Fig. 7 Typical examples of (**a**) $r_{b\bar{b}}$, (**b**) $r_{c\bar{c}}$, and (**c**) r_{gg} distributions

The r_s values were determined by a binned log likelihood fit, where each bin probability is given by Eq. (3). On the basis of the three-dimensional (3D) histogram, 5000 toy MC events were generated using the Poisson distribution function for each bin, which were then fitted to obtain $r_{b\bar{b}}$, $r_{c\bar{c}}$, and r_{gg}. The number of bins in the 3D histogram were optimized to minimize the statistical fluctuation in the fitted results caused by bins with low-statistic. Bins with fewer than one entry were not used for the fitting. The distributions of $r_{b\bar{b}}$, $r_{c\bar{c}}$, and r_{gg} from the template fitting of 5000 toy MC events are shown in Fig. 7. The error in r_s is determined by Gaussian fittings to these distributions, the results of which are shown in Tables 4 and 5 for CM energies of 250 and 350 GeV.

The tables also show the accuracies after correction of the total cross section. From a study of the recoil mass in the process of $e^+e^- \to eeH$ and $\mu\mu H$, the accuracy of the total cross section $(\Delta\sigma/\sigma)$ was estimated to be 2.5 % at 250 GeV [10, 27]. For 350 GeV, we assumed an accuracy of 3.5 % because the recoil mass measurement relies on the ZH process, whose cross section is inversely proportional to the square of the CM energy; thus, the accuracy of the total cross section measurement would be inversely proportional to the CM energy.

From Tables 4 and 5, we see that the Higgs cross section times branching ratio can be measured with a precision of around 1 % for $H \to b\bar{b}$ and 7 to 9 % for $H \to c\bar{c}$ and gg. The measurement is approximately 10–20 % better at 350 GeV than at 250 GeV. The instantaneous luminosity at 350 GeV is 25 % greater than that at 250 GeV according to the ILC beam parameters used in this study. Thus, for an equal running time, measurements at 350 GeV will give about 20–30 % better accuracy than those at 250 GeV. On the other hand, the accuracy of the BR to $b\bar{b}$, $\Delta BR/BR(H \to b\bar{b})$, is limited by the uncertainty on the total cross section; measurement at 250 GeV therefore gives better results than that at 350 GeV. In the other decay channels, comparable BR measurements are possible if the same integrated luminosities are assumed.

5 Conclusion

The accuracies at which the Higgs branching ratios $H \to b\bar{b}$, $c\bar{c}$, and gg can be measured were evaluated at $\sqrt{s} =$ 250 GeV and 350 GeV. In terms of signal significance, $\sqrt{s} = 350$ GeV yields better background suppression than $\sqrt{s} = 250$ GeV in each channel. The combined results for the measurement accuracies of the Higgs cross section times BRs ($\Delta(\sigma \cdot BR)/\sigma \cdot BR$) to $H \to b\bar{b}$, $c\bar{c}$, and gg are 1.0 %, 6.9 %, and 8.5 % at CM energies of 250 GeV and 1.0 %, 6.2 %, and 7.3 % at 350 GeV, assuming the same integrated luminosity of 250 fb^{-1}.

At the ILC, the total Higgs cross-section σ is measured using the Z recoil mass process. Assuming that $\Delta\sigma/\sigma =$ 2.5 % for 250 GeV and assuming it is 3.5 % at 350 GeV, Higgs BRs ($\Delta BR/BR$) to $b\bar{b}$, $c\bar{c}$, and gg are derived as 2.7 %, 7.3 %, and 8.9 % at CM energies of 250 GeV and as 3.6 %, 7.2 %, and 8.1 % at 350 GeV.

We therefore conclude that, assuming equal integrated luminosities at the two CM energies, the Higgs cross section times BR ($BR \times \sigma$) can be measured better at 350 GeV than at 250 GeV owing to the higher S/N at the higher energy. However, when the accuracy of the total cross section measurement by recoil mass measurement is considered, the $H \to b\bar{b}$ BR can be measured better at 250 GeV.

Acknowledgement The authors thank the members of the ILC physics subgroup for useful discussions on this work and those of the ILD software and optimization group, who maintain the software and MC samples used in this work. We are especially grateful to Tomohiko Tanabe, Keisuke Fujii, and Daniel Jeans for their valuable comments to the draft. This work was supported in part by Creative Scientific Research Grant No. 18GS0202 from the Japan Society for Promotion of Science (JSPS), the JSPS Core University Program, and JSPS Grant-in-Aid for Scientific Research No. 22244031.

References

1. A. Droll, H.E. Logan, Phys. Rev. D **76**, 015001 (2007)
2. DELPHI, ALEPH, L3, OPAL Collaborations, Phys. Lett. B **565**, 61 (2003)
3. CDF, D0 Collaborations, Phys. Rev. Lett. **104**, 061802 (2010), update is obtained as arXiv:1207.0449v2 [hep-ex]
4. The ATLAS Collaboration, Phys. Lett. B **710**, 49 (2012)
5. The CMS Collaboration, Phys. Lett. B **710**, 26 (2012)
6. M. Carena, H. Haber, H. Logan, S. Mrenna, Phys. Rev. D **65**, 055005 (2002)
7. M. Battaglia, arXiv:hep-ph/9910271
8. J. Kamoshita, Y. Okada, M. Tanaka, Phys. Lett. B **391**, 124 (1997)
9. I. Nakamura, K. Kawagoe, Phys. Rev. D **54**, 3634 (1996)
10. ILD Concept Group, The International Large Detector: letter of intent. arXiv:1006.3396v1 [hep-ex]
11. SiD Concept Group, SiD letter of intent. arXiv:0911.0006v1 [physics.ins-det]
12. T. Kuhl, K. Desch, LC-PHSM-2007-001 (2007)
13. J.-C. Brient, LC-PHSM-2002-003 (2002)
14. Y.G. Bong et al., J. Korean Phys. Soc. **50**, 10–17 (2007)
15. Y. Banda, T. Lastovicka, A. Nomerotski, Phys. Rev. D **82**, 033013 (2010)
16. W. Kilian et al., arXiv:0708.4233 [hep-ph]
17. M. Moretti et al., arXiv:hep-ph/0102195v1
18. T. Sjöstrand, S. Mrenna, P. Skands, J. High Energy Phys. **0605**, 026 (2006)
19. M.A. Thomson, Nucl. Instrum. Methods Phys. Res., Sect. A **611**, 25–40 (2009)
20. S. Agostinelli et al. (GEANT4 Collaboration), Nucl. Instrum. Methods Phys. Res., Sect. A **506**, 250 (2003)
21. P. Mora de Freitas, H. Videau, LC-TOOL-2003-010, Prepared for LCWS 2002, Jeju Island, Korea, 26–30 August 2002
22. O. Wendt, F. Gaede, T. Krämer, arXiv:physics/0702171v1 [physics.ins-det]
23. K. Fujii, T. Matsui, Y. Sumino, Phys. Rev. D **50**, 4341 (1994)
24. A. Djouadi et al., International Linear Collider reference design report volume 2: PHYSICS AT THE ILC. arXiv:0709.1893v1 [hep-ph]
25. J. Brau et al., The International Linear Collider interim report volume 2, physics and detectors 2011 status report, KEK report 2011-5
26. D. Bailey et al., Nucl. Instrum. Methods Phys. Res., Sect. A **610**, 2 (2009)
27. H. Li, arXiv:1007.2999v1 [hep-ex]